

Sahy, D., Hiess, J., Fischer, A.U., Condon, D.J., Terry, D.O., Jr., Abels, H.A., Hüsing, S.K., and Kuiper, K.F., 2019, Accuracy and precision of the late Eocene–early Oligocene geomagnetic polarity time scale: GSA Bulletin, <https://doi.org/10.1130/B35184.1>.

Data Repository

Figure S1. Results of high-field thermomagnetic runs in air using a modified horizontal translation type Curie balance (Mullender et al., 1993) with a sensitivity of $\sim 5 \times 10^{-9}$ Am². For each run, 50–80 mg of powdered sample was held in a quartz sample holder and placed inside a cycling magnetic field that varied between 100–300 mT. Analysis over different heating and cooling cycles performed at a rate of 10°C/min to a maximum temperature of 700 °C showed the destruction of a mineral phase up to 560–600 °C indicating the presence of iron oxides, such as magnetite, as the main carrier of remanent magnetisation. Tc—Curie temperature.

Table S1. Location of sections sampled for paleomagnetic analysis at Flagstaff Rim.

Table S2. Location of sections sampled for paleomagnetic analysis at Toadstool Geologic Park (note that there is no section TGP_S11 in the record).

Table S3. Results of paleomagnetic analysis of samples from Flagstaff Rim.

Table S4. Results of paleomagnetic analysis of samples from Toadstool Geologic Park.

Table S5. Summary of magnetic reversal ages and associated uncertainties from the WRG, UMB, ATPS06 and PEAT records.

Supplement to: Accuracy and precision of the late Eocene – early Oligocene geomagnetic polarity time scale by Sahy, D., Hiess, J., Fischer, A., Condon, D.J., Terry, D.O. Jr., Abels, H.A., Hüsink, S.K., and Kuiper, K.F.

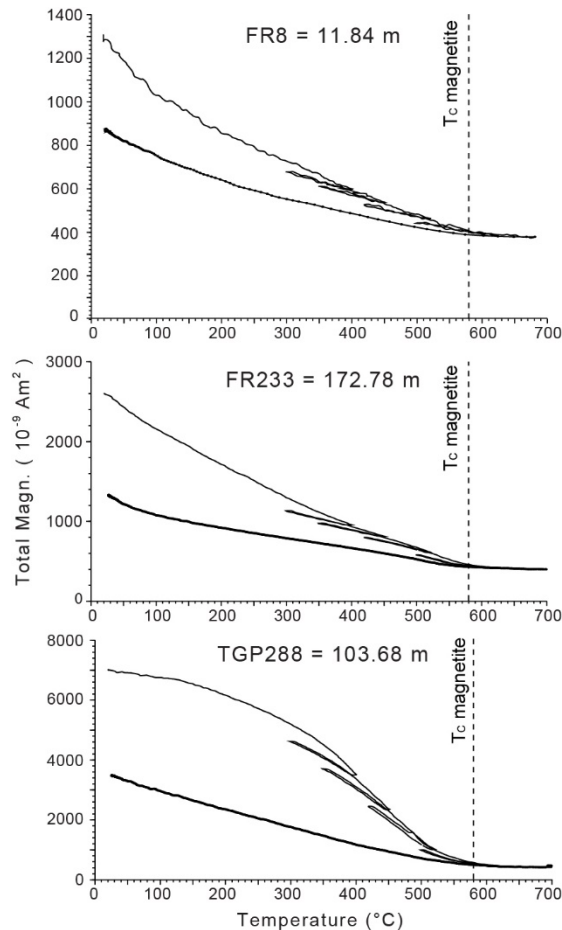


Figure S1 Results of high-field thermomagnetic runs in air using a modified horizontal translation type Curie balance (Mullender et al., 1993) with a sensitivity of $\sim 5 \times 10^{-9}$ Am². For each run, 50–80 mg of powdered sample was held in a quartz sample holder and placed inside a cycling magnetic field that varied between 100–300 mT. Analysis over different heating and cooling cycles performed at a rate of 10°C/min to a maximum temperature of 700°C showed the destruction of a mineral phase up to 560–600°C indicating the presence of iron oxides, such as magnetite, as the main carrier of remanent magnetisation. Tc – Curie temperature.

S1. $^{206}\text{Pb}/^{238}\text{U}$ calibrated age model for the White River Group

Age–depth models for the Flagstaff Rim and TGP sedimentary successions were developed by Sahy et al. (2015) based on zircon $^{206}\text{Pb}/^{238}\text{U}$ dates from 15 volcanic tuffs, using the Bayesian approach implemented in the P_Sequence routine of the OxCal 4.2 software package (Bronk-Ramsey, 2008). This approach treats sediment accumulation as a random Poisson process, where sediment beds of finite thickness are deposited at discrete points in time and are separated by gaps of variable

duration, approximating the processes that lead to sediment accumulation in a fluvial environment. The uncertainty envelopes calculated using this approach vary in width, narrowing in the vicinity of radio-isotopically dated tie-points and a widening as distance from the nearest tie-point increases. The resulting uncertainty envelopes are wider than those typically obtained using conventional linear or polynomial interpolation, but the dates are likely to be more accurate. Additionally, the flexibility of the P_Sequence model allows for the integration of radio-isotopic data with the position of lithological boundaries, which are likely to correspond to changes in sediment accumulation rates. The stratigraphic resolution of the model, i.e. the thicknesses of deposits resulting from individual accumulation events is set by the user through an input parameter k , defined as the number of accumulation events per unit depth, with higher/lower values corresponding to finer/coarser sediments and continuous/episodic sedimentation (Bronk Ramsey, 2008). Because selecting the right k value for a given sedimentary succession is difficult, and an unsuitable value would lead to an unrealistically precise age model, the user may specify a nominal k value (k_0) and an associated *a priori* probability density function, such that output data are an aggregate of simulations run over a range of possible k values. Input data for the FR and TGP age depth model were described in detail by Sahy et al. (2015). For the FR succession the model was based on the $^{206}\text{Pb}/^{238}\text{U}$ age of the B, B+15, B+18, F-7, F, G, H, J-1 and J tuffs, with a change in sedimentation rate constrained to occur at the level of the I tuff, corresponding to a shift from fluvial towards eolian sedimentation. The model was run with a nominal k value of 10, which was allowed to vary uniformly over two orders of magnitude each way, and resulted in an agreement index of 97.4%, indicating that the prior and posterior PDFs of the input parameter are consistent with each other.

Input data for the TGP record consisted of the weighted mean $^{206}\text{Pb}/^{238}\text{U}$ age of the TP-1, TP-2, UPW, Serendipity, and Lower and Upper Whitney Ashes, and the stratigraphic position of the contact between the Chadron and Brule Formations at 48.25 m, and between the Orella and Whitney Members of the Brule Formation at 90.25 m. Because initial k parameter values identical to those used for the Flagstaff Rim record did not yield stable results, the model was run with a nominal value

of k0=10 and a narrower uniform PDF of lg(k/k0)=(-1,1) resulting in an overall agreement index of 98.4%.

S2. Uncertainty propagation

Age control for the magnetic reversals recorded in the WRG and UMB successions is based on the $^{206}\text{Pb}/^{238}\text{U}$ dating of zircons from volcanic tuffs. Uncertainties associated with radio-isotopic dating are typically approximated by a normal distribution – thus it is assumed that the ‘true’ value is more likely to lie near the nominal value than at the outer limits of the 95% confidence interval. The same can be said for uncertainties associated with the ^{238}U decay constant (ca. 0.11%) and the calibration of the isotopic tracers used in $^{206}\text{Pb}/^{238}\text{U}$ dating (ca. 0.03%). Consequently a reasonable approximation of the age uncertainty of an interpolated $^{206}\text{Pb}/^{238}\text{U}$ dated magnetic reversal can be obtained by adding these uncertainties in quadrature:

$$\sigma_{\text{Age U-Pb}} = \sqrt{\sigma_{\text{U-Pb model}}^2 + \sigma_{\lambda_{238\text{U}}}^2 + \sigma_{\text{Tracer}}^2} \quad (\text{Equation S1})$$

where $\sigma_{\text{Age U-Pb}}$ is the age uncertainty associated with a U-Pb calibrated magnetic reversal, $\sigma_{\text{U-Pb model}}$ is the output from the OxCal age-depth model discussed in Section S1, which takes into account analytical uncertainties associated with the underpinning U-Pb dates, $\sigma_{\lambda_{238\text{U}}}$ is the systematic uncertainty associated with the ^{238}U decay constant, and σ_{Tracer} is the systematic uncertainty associated with the synthetic U-Pb isotopic tracer. Similarly, if astronomically tuned ages are assumed to carry a systematic uncertainty of 0.1% characteristic of the 405 kyr eccentricity cycle in the Paleogene, then the age uncertainty of an astronomically tuned magnetic reversal becomes:

$$\sigma_{\text{Age astro}} = \sqrt{\sigma_{\text{astro model}}^2 + \sigma_{405 \text{ kyr}}^2} \quad (\text{Equation S2})$$

where $\sigma_{\text{Age astro}}$ is the age uncertainty associated with an astronomically tuned magnetic reversal, $\sigma_{\text{astro model}}$ is the uncertainty associated with the tuning process estimated at ± 50 kyr for the ATPS06 and the PEAT, and $\sigma_{405 \text{ kyr}}$ is the systematic uncertainty associated with the 405 kyr eccentricity cycle.

By convention, the stratigraphic position of a magnetic reversal is assumed to lie halfway between consecutive samples of opposite polarity. However the position of the respective samples is determined by the stratigraphic resolution at which the record was sampled, and consequently there is no compelling reason to assume that the reversal is more likely to lie close to the midpoint of this interval than nearer its outer bounds. It follows that this stratigraphic uncertainty is more appropriately modelled by a uniform distribution, in which case the total uncertainty of an interpolated $^{206}\text{Pb}/^{238}\text{U}$ dated or astronomically tuned magnetic reversal is:

$$\sigma_{Total\ U-Pb} = \sigma_{Age\ U-Pb} + \sigma_{Strat} \quad (\text{Equation S3})$$

$$\sigma_{Total\ Astro} = \sigma_{Age\ astro} + \sigma_{Strat} \quad (\text{Equation S4})$$

where σ_{strat} is the stratigraphic uncertainty converted to Myr based on mean sediment accumulation rates.

When assessing discrepancies between the WRG and UMB records, systematic $^{206}\text{Pb}/^{238}\text{U}$ uncertainties need not be considered, and so the uncertainty on the age offset between magnetic reversals from these records is quantified as:

$$\sigma_{\Delta t\ WRG-UMB} = \sqrt{\sigma_{U-Pb\ model_{WRG}}^2 + \sigma_{U-Pb\ model_{UMB}}^2 + \sigma_{Strat_{WRG}}^2 + \sigma_{Strat_{UMB}}^2} \quad (\text{Equation S5})$$

When comparing magnetic reversal ages from the WRG to the astronomically tuned ATPS06 and PEAT records the systematic sources of uncertainty relevant to each method must also be taken into account, and the uncertainty on the age offset between different age models is calculated as:

$$\sigma_{\Delta t\ WRG-astro} = \sqrt{\sigma_{U-Pb\ model_{WRG}}^2 + \sigma_{astro\ model}^2 + \sigma_{\lambda_{238U}}^2 + \sigma_{Tracer}^2 + \sigma_{405\ kyr}^2 + \sigma_{Strat_{WRG}}^2 + \sigma_{Strat_{astro}}^2} \quad (\text{Equation S6})$$

When using U-Pb calibrated or astronomically tuned magnetic reversal ages to assess seafloor spreading rates, uncertainties associated with the duration of each chron, and its width in the South Atlantic anomaly profile of Cande and Kent (1992) must be taken into account. However, if both the top and base of a given chron are dated using the same techniques, then systematic uncertainties associated with that technique need not be considered. The uncertainty associated with the duration of a chron may then be calculated as:

$$\sigma_{duration (U-Pb)} = \sqrt{\sigma_{U-Pb\ model\ (top)}^2 + \sigma_{U-Pb\ model\ (base)}^2} + \sigma_{Strat\ (top)} + \sigma_{Strat\ (base)}$$

(Equation S7)

for U-Pb dated records and:

$$\sigma_{duration (astro)} = \sqrt{\sigma_{astro\ model\ (top)}^2 + \sigma_{astro\ model\ (base)}^2} + \sigma_{Strat\ (top)} + \sigma_{Strat\ (base)}$$

(Equation S8)

for astronomically tuned records. The total uncertainty on the spreading rate (in %) was then calculated by adding the percent uncertainty on the duration of the chron to the percent uncertainty in the width of the same chron based on Table 4 of Cande and Kent (1992):

$$\sigma_{spreading\ rate\ (\%)} = \sigma_{duration\ (\%)} + \sigma_{width\ (\%)} \quad (\text{Equation S9})$$

Section	Thickness (m)	Samples	Base (m)	Base (coordinates)	Top (m)	Top (coordinates)	Correlation to next section
FR_S2	4.76	FR19 - FR25	0	42°38.343'N/106°44.886W	4.76	42°38.342'N/106°44.880W	Sandstone at top of section traced over ~20m
FR_S1	13.69	FR1 - FR18	4.76	42°38.354'N/106°44.876W	18.45	42°38.353'N/106°44.861W	Base of Tuff B traced over ~600 m
FR_S3	8.37	FR26 - FR41	18.74	42°38.388'N/106°45.343W	27.11	42°38.378'N/106°45.351W	Sandstone traced over ~20m
FR_S4	3.12	FR42 - FR49	27.11	42°38.375'N/106°45.340W	30.23	42°38.372'N/106°45.341W	Measured point using Jacob staff and Abney level
FR_S5	4.90	FR50 - FR60	30.23	42°38.397'N/106°45.382W	35.13	42°38.391'N/106°45.382W	Sandstone at top of section traced over ~250m
FR_S6	19.64	FR61 - FR82	36.55	42°38.507'N/106°45.478W	56.19	42°38.524'N/106°45.497W	Base of Tuff F-22 traced over ~500m (prominent dark coloured tuff)
FR_S7	4.14	FR83 - FR88	56.34	42°38.751'N/106°45.554W	60.84	42°38.755'N/106°45.559W	Top of Tuff F-19 traced over ~20m
FR_S8	18.60	FR89 - FR120	60.13	42°38.751'N/106°45.574W	78.73	42°38.771'N/106°45.592W	Base of Tuff F traced over ~250m
FR_S9	7.97	FR121 - FR145	70.76	42°38.648'N/106°45.668W	78.73	42°38.654'N/106°45.675W	Base of Tuff F traced over ~250m (partially duplicates FR_S8 to locate Tuff F-7.5)
FR_S10	18.97	FR146 - FR187	79.05	42°38.670'N/106°45.688W	98.02	42°38.681'N/106°45.708W	Base of Tuff G traced over ~700m
FR_S12	10.36	FR261 - FR282	97.52	42°38.301'N/106°45.775W	107.88	42°38.291'N/106°45.781W	Sandstone at top of section traced over ~10m
FR_S13	3.55	FR283 - FR289	108.18	42°38.291'N/106°45.791W	111.73	42°38.296'N/106°45.804W	Sandstone at top of section traced over ~30m
FR_S14	6.92	FR290 - FR304	111.73	42°38.312'N/106°45.814W	118.65	42°38.312'N/106°45.820W	Sandstone at top of section traced over ~10m
FR_S15	7.18	FR305 - FR321	118.65	42°38.312'N/106°45.822W	125.83	42°38.310'N/106°45.829W	Sandstone at top of section traced over ~20m
FR_S16	4.65	FR322 - FR331	125.83	42°38.320'N/106°45.833W	130.48	42°38.318'N/106°45.838W	Sandstone at top of section traced over ~10m
FR_S17	3.49	FR332 - FR342	130.63	42°38.321'N/106°45.841W	134.13	42°38.319'N/106°45.845W	Sandstone traced over ~10m
FR_S18	4.03	FR343 - FR351	135.45	42°38.324'N/106°45.850W	139.48	42°38.321'N/106°45.854W	Sandstone at top of section traced over ~10m
FR_S19	4.43	FR352 - FR359	140.18	42°38.329'N/106°45.856W	144.61	42°38.326'N/106°45.861W	Sandstone at top of section traced over ~10m
FR_S20	6.16	FR360 - FR369	144.61	42°38.333'N/106°45.862W	150.77	42°38.333'N/106°45.865W	Sandstone at top of section traced over ~10m
FR_S21	7.99	FR370 - FR374	150.77	42°38.326'N/106°45.866W	158.76	42°38.328'N/106°45.871W	Base of Tuff H traced over ~400m
FR_S11	24.56	FR217 - FR260	158.76	42°38.510'N/106°45.777W	183.52	42°38.497'N/106°45.836W	

Table S1 Location of sections sampled for paleomagnetic analysis at Flagstaff Rim. Latitude and longitude reported relative to WGS84. Base and Top refer to the position of the sampled interval in the composite Flagstaff Rim record. The base of the Flagstaff Rim composite is situated 18.35 m below the base of the B Tuff.

Section	Thickness (m)	Samples	Base (m)	Base (coordinates)	Top (m)	Top (coordinates)	Correlation to next section
TGP_S7	2.15	TGP79 – TGP83	0	42°51.814'N/103°34.617'W	2.15	42°51.814'N/103°51.814'W	Limestone traced over ~350m
TGP_S6	1.08	TGP77 – TGP78	2.15	42°51.716'N/103°34.852'W	3.23	42°51.717'N/103°34.854'W	Limestone at top of section traced over ~5m
TGP_S5	2.45	TGP69 – TGP76	2.80	42°51.720'N/103°34.852'W	5.25	42°51.721'N/103°34.855'W	Base of Tuff TP-1 traced over ~10m
TGP_S4	4.47	TGP52 – TGP68	5.10	42°51.725'N/103°34.854'W	9.57	42°51.726'N/103°34.856'W	White bed near top of section traced over ~600m
TGP_S3	1.23	TGP46 – TGP51	8.76	42°51.630'N/103°35.305'W	9.99	42°51.635'N/103°35.301'W	Top of green bed near top of section traced over ~30m
TGP_S2	5.43	TGP24 – TGP45	9.99	42°51.650'N/103°35.314'W	15.42	42°51.653'N/103°35.318'W	Top of green bed near top of section traced over ~100m
TGP_S1	8.16	TGP1 – TGP23	14.82	42°51.643'N/103°35.389'W	22.98	42°51.636'N/103°35.391'W	White layer near top of section traced over ~50m
TGP_S8	7.52	TGP84 – TGP103	22.63	42°51.661'N/103°35.394'W	30.15	42°51.657'N/103°35.409'W	Lower Purplish White Layer traced over ~10m
TGP_S9	8.36	TGP104 – TGP126	30.15	42°51.651'N/103°35.410'W	38.25	42°51.657'N/103°35.417'W	Upper Purplish White Layer traced over ~1km.
TGP_S13	6.96	TGP171 – TGP200	37.10	42°51.246'N/103°34.990'W	44.06	42°51.241'N/103°34.989'W	Brown bed traced over ~10m
TGP_S12	4.45	TGP164 – TGP170	44.06	42°51.244'N/103°34.979'W	48.51	42°51.226'N/103°34.981'W	Lowermost Orella sandstone traced over ~70m
TGP_S10	11.13	TGP127 – TGP163	48.51	42°51.240'N/103°35.021'W	59.64	42°51.225'N/103°35.029'W	Horus ash identified here and at location of section TGP_S14
TGP_S14	2.60	TGP201 – TGP208	59.64	42°51.133'N/103°35.297'W	62.24	42°51.131'N/103°35.294'W	Sandstone traced over ~100m
TGP_S16	1.77	TGP214 – TGP218	62.24	42°51.129'N/103°35.393'W	64.01	42°51.129'N/103°35.386'W	Sandstone traced over ~10m
TGP_S15	1.89	TGP209 – TGP213	64.01	42°51.123'N/103°35.394'W	65.90	42°51.126'N/103°35.387'W	Sandstone traced over ~10m
TGP_S17	1.73	TGP219 – TGP221	65.00	42°51.129'N/103°35.387'W	66.73	42°51.128'N/103°35.387'W	Sandstone traced over ~170m
TGP_S18	3.00	TGP222 – TGP228	66.02	42°51.048'N/103°35.452'W	69.02	42°51.043'N/103°35.453'W	Sandstone traced over ~20m
TGP_S19	9.70	TGP229 – TGP245	69.02	42°51.039'N/103°35.462'W	78.72	42°51.024'N/103°35.459'W	Green layer traced over ~400m
TGP_S20	6.77	TGP246 – TGP256	78.62	42°50.848'N/103°35.542'W	85.39	42°50.846'N/103°35.549'W	Sandstone traced over ~300m
TGP_S21	2.56	TGP257 – TGP261	84.81	42°50.752'N/103°35.414'W	87.37	42°50.754'N/103°35.416'W	Uppermost Orella sandstone traced over 70m
TGP_S22	7.12	TGP262 – TGP275	88.62	42°50.750'N/103°35.376'W	95.74	42°50.744'N/103°35.366'W	Green layer traced over ~100 m
TGP_S23	21.34	TGP276 – TGP305	95.34	42°50.750'N/103°35.267'W	116.68	42°50.492'N/103°35.107'W	Lower Whitney Ash traced over ~200m
TGP_S24	24.57	TGP306 – TGP335	116.68	42°50.384'N/103°35.077'W	141.25	42°50.109'N/103°35.104'W	

Table S2 Location of sections sampled for paleomagnetic analysis at Toadstool Geologic Park (note that there is no section TGP_S11 in the record). Latitude and longitude reported relative to WGS84. Base and Top refer to the position of the sampled interval in the composite Toadstool Geologic Park record. The base of the Toadstool Geologic Park composite is situated 38.25 m below the base of the Upper Purplish White Layer.

Table S3 Results of paleomagnetic analysis of samples from Flagstaff Rim. Metre level indicates the sample's position in the FR composite section. Section labels match those listed in Table S1. Demagnetization method indicates whether the high-temperature magnetic component was obtained via thermal (th) or alternating field (af) demagnetization. The low-temperature component was calculated based on three consecutive steps of thermal demagnetization up to 200-240°C. Min/max indicate the first/last demagnetization step included in the high-temperature magnetic component - plain text indicates temperature for thermal demagnetization, numbers in italics indicate alternating field intensity. MAD - mean angular deviation. VGP - virtual geomagnetic pole, n - number of demagnetisation steps included in the high-temperature component. For notes on sample quality categories see Section 4.1. Category A samples, used in establishing the magnetic polarity pattern of the TGP record, are listed in bold.

Sample	m level	Section	Demag. method	Quality	Low temperature component			High temperature component							
					Declinatio	Inclinatio	MAD	min.	max.	n	Declinatio	Inclinatio	MAD	VGP lon	VGP lat
FR25	0.57	FR_S2	th	D	342.1	66.2	16.8	-	-	-	-	-	-	-	-
FR23	1.51	FR_S2	af	D	324.5	42.8	8.9	-	-	-	-	-	-	-	-
FR22	2.45	FR_S2	th	C	336.0	58.3	7.8	330	390	3	181.7	81.5	28.7	252.7	26
FR21	3.22	FR_S2	af	A	10.4	36.3	17.2	30	70	11	11.0	72.1	7.6	275.1	73.9
FR19	4.26	FR_S2	th	A	325.5	30.4	12.8	270	420	4	313.4	37.3	18.3	148.9	45.5
FR17	4.99	FR_S1	af	A	18.8	69.2	10.0	5	40	7	346.0	64.0	5.1	185.2	79.5
FR16	5.45	FR_S1	af	A	24.3	60.6	3.9	270	25	5	38.0	63.0	7.8	326.1	62.6
FR12	8.05	FR_S1	th	A	44.9	20.0	4.9	270	330	3	334.6	50.0	12.7	141.3	66
FR11	9.37	FR_S1	af	A	18.0	62.7	14.8	5	100	11	358.4	35.0	12.4	77	66.7
FR10	10.18	FR_S1	th	A	10.3	69.9	2.3	300	450	7	35.9	61.6	10.5	330.5	63.8
FR9	10.87	FR_S1	af	A	19.9	70.7	4.1	270	15	3	350.2	82.1	6.2	248.3	57.8
FR8	11.84	FR_S1	th	A	293.2	54.2	4.0	270	450	5	346.8	34.8	17.3	102.7	64
FR7	12.60	FR_S1	af	A	161.9	86.9	12.3	35	60	4	314.4	64.3	8.3	185.4	57.5
FR6	13.26	FR_S1	th	A	15.7	65.9	1.1	270	390	5	357.5	68.9	9.3	244.3	80.1
FR4	14.72	FR_S1	th	A	30.7	63.9	6.8	270	420	5	312.8	71.9	10.3	205.4	57.2
FR3	15.21	FR_S1	af	A	48.2	35.3	1.0	5	50	9	19.4	70.0	4.3	294.9	72.9
FR2	15.83	FR_S1	af	A	16.6	54.4	6.4	270	20	3	44.6	60.3	3.5	330.1	57.2
FR1	16.10	FR_S1	th	D	-	-	-	-	-	-	-	-	-	-	-
FR29	20.56	FR_S3	af	A	25.0	74.8	12.6	10	70	8	353.2	73.8	8.3	241.9	72.3
FR30	21.06	FR_S3	th	D	30.9	61.7	5.4	-	-	-	-	-	-	-	-
FR33	22.80	FR_S3	af	A	302.1	32.6	15.8	270	40	6	33.7	54.2	16.1	348.6	62.7
FR34	23.31	FR_S3	af	A	185.9	77.8	8.9	270	25	5	342.1	16.5	5.3	103.1	52.4
FR36	24.11	FR_S3	th	D	2.8	78.6	4.6	-	-	-	-	-	-	-	-
FR37	24.58	FR_S3	th	A	352.9	70.2	8.6	280	460	5	351.2	77.9	11.4	249.9	65.3
FR38	24.93	FR_S3	af	B	7.3	78.7	15.1	240	40	5	282.8	-27.8	18.0	143.8	-0.9
FR39	25.50	FR_S3	af	A	8.2	74.1	17.5	35	70	5	352.4	33.7	10.0	90.5	65
FR40	25.89	FR_S3	th	D	327.3	63.2	6.2	-	-	-	-	-	-	-	-
FR41	26.52	FR_S3	af	A	28.3	52.2	21.4	270	10	3	319.4	60	7.8	173.9	60
FR42	27.42	FR_S4	th	A	25.0	53.5	7.6	10	20	3	238.6	-24	14.0	175.7	-31.4
FR43	27.73	FR_S4	th	D	33.3	56.8	5.1	-	-	-	-	-	-	-	-
FR44	27.88	FR_S4	th	C	56.3	81.7	11.6	280	460	3	234.1	75	27.3	228.6	23.1

FR125	77.82	FR_S9	th	C	339.2	70.9	7.8	280	520	3	216.3	-35	25.8	189.1	-51.6
FR123	78.63	FR_S9	th	C	10.2	66.6	5.7	240	620	3	180.8	-38.4	31.1	251.1	-69
FR122	78.73	FR_S9	af	B	12.7	21.7	16.2	270	60	5	112.6	-17.4	15.0	334.3	-22.6
FR147	79.48	FR_S10	af	B	32.5	60.0	23.2	270	20	4	205.8	48.2	9.9	230.1	-14.4
FR149	80.23	FR_S10	af	D	30.8	32.1	12.9	-	-	-	-	-	-	-	-
FR154	82.34	FR_S10	th	B	344.9	72.6	17.6	240	480	6	258.6	-13.1	14.7	166	-12.9
FR157	83.33	FR_S10	af	D	6.0	48.8	12.7	-	-	-	-	-	-	-	-
FR159	84.13	FR_S10	th	D	24.2	74.1	8.7	-	-	-	-	-	-	-	-
FR161	85.00	FR_S10	af	A	12.2	66.8	6.7	200	60	11	145.1	-49.6	14.8	331.1	-59.7
FR162	85.28	FR_S10	af	A	21.4	66.3	5.4	25	40	4	163.6	62.2	14.4	353	-78
FR168	87.04	FR_S10	af	A	46.6	50.9	12.0	270	50	8	162.5	-80.5	13.9	62.2	-59.8
FR169	87.37	FR_S10	af	A	355.6	56.9	5.4	10	100	11	174.4	-81.5	4.9	70.1	-59.1
FR171	87.99	FR_S10	th	D	29.6	45.5	6.4	-	-	-	-	-	-	-	-
FR172	88.41	FR_S10	af	A	305.7	75.2	12.5	35	70	5	176	-55.2	7.1	278.8	-82.5
FR173	88.81	FR_S10	af	A	332.0	75.0	12.7	20	100	11	183.4	-67.4	8.3	89-1	-82
FR175	89.01	FR_S10	af	B	13.2	37.0	3.4	15	70	7	57.5	-46	11.8	24.6	2.3
FR177	89.73	FR_S10	th	D	334.2	65.2	13.1	-	-	-	-	-	-	-	-
FR178	90.44	FR_S10	af	A	15.1	65.5	5.6	270	70	10	158.7	-53.1	13.6	322.1	-71.1
FR179	90.89	FR_S10	af	A	306.1	62.4	8.4	40	100	5	186.1	-40.6	18.8	236.6	-69.9
FR180	91.36	FR_S10	th	D	11.9	65.0	6.9	-	-	-	-	-	-	-	-
FR183	92.98	FR_S10	af	A	357.6	59.0	6.6	270	80	13	168.7	-61.3	12.9	345.7	-81.7
FR184	93.24	FR_S10	af	A	355.4	53.7	5.7	30	90	5	168.8	-51.7	13.6	297.7	-76.4
FR186	93.88	FR_S10	af	D	2.3	68.2	5.1	-	-	-	-	-	-	-	-
FR187	94.93	FR_S10	th	D	351.4	55.0	3.1	-	-	-	-	-	-	-	-
FR188	95.31	FR_S10	af	B	327.1	53.1	21.6	35	80	4	354.3	-55.5	18.9	77.9	11.2
FR190	96.22	FR_S10	af	D	6.1	55.0	4.7	-	-	-	-	-	-	-	-
FR261	98.33	FR_S12	th	A	155.1	23.0	5.1	280	430	4	166.4	-17.7	9.9	276.7	-54.4
FR263	99.12	FR_S12	th	C	53.0	41.2	1.3	250	400	3	222.2	18	24.7	206	-25.4
FR265	99.87	FR_S12	th	D	333.2	34.5	10.6	-	-	-	-	-	-	-	-
FR267	100.92	FR_S12	th	D	342.1	81.9	6.4	-	-	-	-	-	-	-	-
FR269	101.76	FR_S12	th	A	52.3	46.5	17.0	200	400	5	173.2	-48.3	9.3	277.8	-75.6
FR273	103.85	FR_S12	th	D	310.4	75.0	3.2	-	-	-	-	-	-	-	-
FR275	104.64	FR_S12	th	A	22.6	82.4	11.6	200	280	3	238.6	-24.3	12.9	175.5	-31.5
FR279	106.50	FR_S12	th	A	167.5	44.9	11.9	150	220	3	186.1	-66.3	16.7	105.9	-82.5
FR281	107.46	FR_S12	th	A	334.2	84.8	34.5	280	430	5	203.5	-22.1	16.1	213	-52.8
FR283	108.28	FR_S13	th	A	302.7	66.0	22.2	200	280	4	168.1	-32.9	10.2	279.1	-63.3
FR285	109.19	FR_S13	th	D	26.9	73.0	15.7	-	-	-	-	-	-	-	-
FR287	109.91	FR_S13	th	A	333.1	67.4	5.2	250	430	7	165.7	-28.2	9.6	281.5	-59.8
FR289	110.78	FR_S13	th	D	17.0	73.4	10.1	-	-	-	-	-	-	-	-
FR291	112.13	FR_S14	th	A	37.2	45.1	42.0	150	310	7	183.5	-53.5	5.3	234.3	-81
FR293	112.78	FR_S14	th	A	345.9	69.8	20.8	200	430	7	181	-58.6	6.1	239.9	-86.6
FR295	113.85	FR_S14	th	A	320.7	63.2	3.1	200	340	5	145	-67.4	12.6	13.1	-65

FR297	114.95	FR_S14	th	A	17.9	64.8	9.2	200	430	8	173.2	-44.4	9.9	274	-72.6
FR300	116.31	FR_S14	th	A	353.7	77.5	19.7	200	310	5	127.5	-44.3	10.4	339.4	-44.4
FR303	117.58	FR_S14	th	A	19.7	-6.1	5.4	220	310	4	208.7	-39.2	17.5	194.6	-58.6
FR304	117.95	FR_S14	th	A	6.8	59.4	4.8	200	310	4	158.6	-39.9	17.1	301.7	-63.3
FR305	119.14	FR_S15	th	A	37.2	74.1	10.2	200	310	5	197.3	-65.4	6.1	135.3	-76.9
FR307	119.75	FR_S15	th	A	-	-	-	200	310	3	143.8	-44.3	18.4	325.6	-56.2
FR308	120.17	FR_S15	th	B	59.6	81.3	19.2	200	340	6	228.6	53.5	7.9	214.8	-1.4
FR311	121.72	FR_S15	th	D	58.8	50.7	8.0	-	-	-	-	-	-	-	-
FR312	122.02	FR_S15	th	A	359.6	76.9	7.4	220	280	3	196	-40.4	18.3	214	-66.4
FR315	123.19	FR_S15	th	A	50.5	64.5	12.7	200	310	5	187	-36.8	7.0	236.1	-67.1
FR318	124.21	FR_S15	th	B	14.4	72.7	4.3	370	520	4	100.3	-46.2	14.5	358.2	-25.4
FR321	125.33	FR_S15	th	D	57.6	63.1	7.6	-	-	-	-	-	-	-	-
FR322	125.84	FR_S16	th	D	12.2	48.3	6.5	-	-	-	-	-	-	-	-
FR325	126.96	FR_S16	th	A	27.5	52.0	13.8	200	310	3	153.1	-86.1	10.9	67.8	-49.4
FR327	127.80	FR_S16	th	A	7.5	66.0	5.7	310	370	3	345.8	66.9	15.1	203.3	78
FR329	128.70	FR_S16	th	D	13.5	78.1	14.7	-	-	-	-	-	-	-	-
FR331	129.59	FR_S16	th	A	354.9	98.1	4.5	280	460	4	352.4	67.8	18.4	223.4	80.3
FR333	130.71	FR_S17	th	A	11.5	70.9	9.1	280	460	5	342	49.9	16.5	129.4	71.4
FR336	131.62	FR_S17	th	C	356.2	70.4	1.5	280	400	3	57.8	69.5	27.3	306.8	51
FR338	132.44	FR_S17	th	A	35.2	78.4	6.5	280	430	8	353.5	66.4	8.3	219.5	82.3
FR341	133.59	FR_S17	th	A	2.2	54.1	5.4	250	520	10	357.8	59.5	9.2	109.9	87.2
FR343	135.45	FR_S18	th	A	305.2	26.9	3.6	280	550	8	321	46.7	7.8	151.1	55.3
FR345	136.52	FR_S18	th	A	104.7	68.9	10.1	280	460	4	87.8	74.9	18.1	290	37.5
FR347	137.32	FR_S18	th	A	71.5	83.5	7.7	280	490	7	37	56.5	8.1	341.7	61.3
FR349	138.07	FR_S18	th	A	35.2	57.5	8.2	280	460	4	21.7	72.9	18.6	286.3	69.2
FR351	138.95	FR_S18	th	A	17.9	61.7	3.2	280	460	8	7.4	52.3	7.0	39.8	78.7
FR353	140.59	FR_S19	th	A	37.6	67.4	7.9	280	370	4	359.1	57.5	14.2	82.2	85.5
FR355	141.69	FR_S19	th	D	111.7	-12.7	2.3	-	-	-	-	-	-	-	-
FR357	142.82	FR_S19	th	A	2.8	68.1	3.5	280	460	5	328.2	70.9	18.5	206	65.9
FR359	143.76	FR_S19	th	A	6.9	67.2	5.8	310	520	4	337.3	61.8	19.4	172.3	73.4
FR360	145.14	FR_S20	th	C	288.5	70.4	9.8	400	550	5	2.2	70	24.0	259.7	78.6
FR362	146.17	FR_S20	th	A	52.8	54.2	7.4	280	400	3	13.5	72.5	11.5	277.8	72.6
FR364	147.35	FR_S20	th	D	14.8	74.9	9.3	-	-	-	-	-	-	-	-
FR366	148.25	FR_S20	th	D	17.2	64.9	1.8	-	-	-	-	-	-	-	-
FR368	149.65	FR_S20	th	A	6.3	61.5	3.6	175	280	5	172.4	-42.9	8.7	275.1	-71.2
FR370	151.98	FR_S21	th	A	318.9	75.0	14.3	175	370	7	221.5	-64.8	11.6	140.6	-60.5
FR372	153.25	FR_S21	th	D	27.6	66.8	11.7	-	-	-	-	-	-	-	-
FR376	156.10	FR_S21	th	D	276.1	49.3	3.9	-	-	-	-	-	-	-	-
FR205	157.05	FR_S11	th	D	18.8	55.3	5.6	-	-	-	-	-	-	-	-
FR207	159.70	FR_S11	th	A	7.4	82.4	15.0	270	520	9	159.1	-31.4	15.1	294.4	-58.8
FR208	160.18	FR_S11	af	A	2.9	64.4	14.6	35	80	6	157.4	-39.8	10.9	303.6	-62.6
FR210	161.08	FR_S11	af	A	223.4	73.9	10.4	35	100	5	179.2	-38.6	14.9	255.3	-69.1

FR211	161.39	FR_S11	af	A	115.0	72.1	22.7	200	10	5	192.3	-30.5	12.2	227.6	-61.8
FR215	163.38	FR_S11	af	A	333.3	49.0	5.0	15	50	8	163.3	-44.8	10.3	298.7	-68.8
FR217	164.72	FR_S11	af	A	343.6	57.1	11.3	25	90	9	157.8	-49.6	3.0	316	-68.5
FR218	165.12	FR_S11	th	A	14.0	40.9	2.5	200	450	6	184.8	-42.1	9.1	239.4	-71.3
FR219	165.60	FR_S11	th	D	27.2	52.4	5.5	-	-	-	-	-	-	-	-
FR220	165.80	FR_S11	af	A	22.4	72.6	8.3	20	70	8	154.8	-38.9	7.1	306.7	-60.6
FR222	167.27	FR_S11	th	D	36.5	81.0	2.4	-	-	-	-	-	-	-	-
FR226	168.67	FR_S11	af	A	0.1	60.0	3.7	5	60	10	344.1	73.7	6.1	228.9	70.3
FR227	169.45	FR_S11	th	A	350.2	55.8	2.3	280	370	3	28.9	59.6	10.5	339.1	68.4
FR228	170.08	FR_S11	af	A	341.3	51.5	5.7	15	90	11	358.9	49.9	6.4	77.8	78.1
FR229	170.65	FR_S11	th	D	339.9	68.1	1.5	-	-	-	-	-	-	-	-
FR230	171.43	FR_S11	af	A	337.8	70.8	3.3	10	35	6	356.2	66.2	4.0	230.6	83.5
FR231	171.82	FR_S11	th	C	25.1	65.5	6.4	280	370	3	283.1	56.5	33.5	184.7	32.8
FR233	172.78	FR_S11	th	A	15.3	70.4	2.6	270	450	6	37.2	70.5	5.6	303.6	63
FR235	174.06	FR_S11	af	A	349.2	65.2	2.3	270	40	8	351.5	68.7	8.7	224.9	78.9
FR237	174.81	FR_S11	th	A	349.7	63.1	6.5	280	490	8	45.3	68.1	8.4	311.5	58.4
FR238	175.31	FR_S11	af	A	5.6	66.7	0.9	10	50	8	356.5	74.8	4.8	248.1	71
FR239	175.71	FR_S11	th	A	12.2	47.1	15.8	270	360	4	3.3	67.9	7.6	267.2	81.4
FR242	175.76	FR_S11	af	A	339.1	68.0	5.7	15	70	8	345.4	69.8	5.5	217.1	75.3
FR245	177.10	FR_S11	th	A	335.5	64.1	3.5	270	390	4	328.4	67.3	15.0	193.3	67.1
FR246	177.36	FR_S11	af	A	33.2	63.7	4.2	15	30	4	330.5	73.7	7.3	216.9	65.2
FR250	178.89	FR_S11	af	A	341.8	73.3	2.0	5	40	8	14.8	73.8	3.2	275.8	70.5
FR251	179.38	FR_S11	th	A	345.8	58.8	2.3	270	480	6	304.3	75.7	17.6	215.3	52.3
FR252	179.81	FR_S11	th	D	10.6	52.9	3.0	-	-	-	-	-	-	-	-
FR253	180.37	FR_S11	th	A	2.8	63.6	3.9	310	400	6	7.4	63.7	8.0	313.5	84
FR255	181.45	FR_S11	af	A	12.9	63.9	4.0	270	50	9	322	76.9	3.6	222.8	59.1
FR256	182.24	FR_S11	th	A	357.7	64.2	4.5	280	400	4	359.4	41.8	18.0	74.9	71.5
FR258	182.50	FR_S11	th	A	2.3	60.3	8.1	270	360	4	288.3	65.1	11.1	194.8	40.8

Table S4 Results of paleomagnetic analysis of samples from Toadstool Geologic Park. Metre level indicates the sample's position in the TGP composite section. Section labels match those listed in Table S2. Demagnetization method indicates whether the high-temperature magnetic component was obtained via thermal (th) or alternating field (af) demagnetization. The low-temperature component was calculated based on three consecutive steps of thermal demagnetization up to 200-240°C. Min/max indicate the first/last demagnetization step included in the high-temperature magnetic component - plain text indicates temperature for thermal demagnetization, numbers in italics indicate alternating field intensity. MAD - mean angular deviation. VGP - virtual geomagnetic pole, n - number of demagnetisation steps included in the high-temperature component. For notes on sample quality categories see Section 4.1. Category A samples, used in establishing the magnetic polarity pattern of the TGP record, are listed in bold.

Sample	m level	Section	Demag method	Quality	Low temperature component			High temperature component					VGP lat	
					Declinatio	Inclinatio	MAD	min	max	n	Declination	Inclinatio	MAD	
TGP83	0.00	TGP_S7	th	D	-	-	-	-	-	-	-	-	-	-
TGP82	0.57	TGP_S7	th	D	5.0	30.6	14.2	-	-	-	-	-	-	-
TGP78	2.25	TGP_S6	af	B	344.3	31.7	11.7	270	15	3	228.7	-36.6	13.7	179.6
TGP74b	3.46	TGP_S5	af	A	0.5	39.0	10.0	270	100	8	356.5	43.5	1.4	87.4
TGP72	4.00	TGP_S5	af	A	322.2	54.1	8.3	200	10	3	133.3	-36.9	9.3	332.3
TGP68	5.10	TGP_S4	af	D	-	-	-	-	-	-	-	-	-	-
TGP67	5.28	TGP_S4	af	B	296.9	61.3	37.5	15	70	6	225.1	-16.4	11.2	194.2
TGP64	6.37	TGP_S4	th	D	56.0	64.1	12.1	-	-	-	-	-	-	-
TGP59	7.70	TGP_S4	af	D	16.0	19.1	10.0	-	-	-	-	-	-	-
TGP58	8.16	TGP_S4	th	D	23.6	55.6	19.6	-	-	-	-	-	-	-
TGP57	8.39	TGP_S4	af	B	14.6	52.6	9.3	270	15	4	45.2	31.7	12.4	6
TGP56	8.69	TGP_S4	af	A	17.2	31.9	11.3	270	80	5	347.6	40.1	13.2	108.3
TGP50	8.97	TGP_S4	af	D	183.6	-13.0	8.0	-	-	-	-	-	-	-
TGP54	9.14	TGP_S4	af	B	14.5	36.2	8.7	10	40	4	238.3	-26.4	11.6	178.1
TGP52	9.57	TGP_S4	th	D	-	-	-	-	-	-	-	-	-	-
TGP48	9.60	TGP_S3	af	D	22.0	-12.7	13.7	-	-	-	-	-	-	-
TGP46	9.82	TGP_S3	af	D	156.3	34.5	4.1	-	-	-	-	-	-	-
TGP43	10.01	TGP_S2	af	D	-	-	-	-	-	-	-	-	-	-
TGP42	10.34	TGP_S2	th	D	-	-	-	-	-	-	-	-	-	-
TGP41	10.60	TGP_S2	th	D	303.5	45.5	14.1	-	-	-	-	-	-	-
TGP39	11.19	TGP_S2	af	A	357.7	49.2	27.3	270	15	4	351.0	46.5	6.8	106
TGP36	11.79	TGP_S2	th	D	-	-	-	-	-	-	-	-	-	-
TGP35	11.94	TGP_S2	af	D	-	-	-	-	-	-	-	-	-	-
TGP33	12.31	TGP_S2	th	D	339.0	56.9	6.0	-	-	-	-	-	-	-
TGP32	12.81	TGP_S2	af	A	347.1	61.9	17.7	5	35	7	304.2	62.2	8.9	187.8
TGP31	13.10	TGP_S2	af	A	-	-	-	270	80	9	335.4	56.3	19.6	158.3
TGP30	13.36	TGP_S2	af	D	-	-	-	-	-	-	-	-	-	-
TGP29	13.63	TGP_S2	af	D	15.0	87.9	11.5	-	-	-	-	-	-	-
TGP28	13.99	TGP_S2	af	D	11.2	73.7	16.3	-	-	-	-	-	-	-
TGP27	14.30	TGP_S2	af	D	7.6	50.8	5.5	-	-	-	-	-	-	-
TGP26	14.74	TGP_S2	af	D	-	-	-	-	-	-	-	-	-	-
TGP25	15.01	TGP_S2	af	D	15.0	58.2	4.7	-	-	-	-	-	-	-
TGP24	15.32	TGP_S2	th	D	116.3	60.1	16.5	-	-	-	-	-	-	-

TGP22b	16.36	TGP_S1	af	A	304.9	-38.7	15.2	270	30	6	126.5	-37.5	10.2	338.3	-40.7
TGP19b	17.25	TGP_S1	af	A	321.0	68.5	20.3	270	30	5	205.3	-38.3	12.1	203.5	-60.2
TGP16	18.45	TGP_S1	af	A	-	-	-	40	70	3	121.1	-36.0	9.9	341.3	-36.1
TGP17	18.45	TGP_S1	af	B	358.4	57.3	3.5	200	20	4	259.0	-27.1	16.6	163.2	-17.7
TGP15	18.76	TGP_S1	af	B	47.6	71.7	21.2	5	20	3	243.5	-49.3	8.2	158.6	-38.6
TGP14	19.09	TGP_S1	th	D	277.2	10.2	20.4	-	-	-	-	-	-	-	-
TGP13	19.66	TGP_S1	af	D	-	-	-	-	-	-	-	-	-	-	-
TGP12	19.98	TGP_S1	af	D	14.0	69.2	15.0	-	-	-	-	-	-	-	-
TGP11	20.32	TGP_S1	af	D	-	-	-	-	-	-	-	-	-	-	-
TGP10	20.67	TGP_S1	th	D	33.1	55.2	14.5	-	-	-	-	-	-	-	-
TGP9	21.02	TGP_S1	af	C	351.1	44.2	15.2	10	40	3	336.7	42.6	23.6	131.3	63.8
TGP8	21.46	TGP_S1	af	C	-	-	-	5	40	3	198.5	-42.3	28.3	210.6	-66.4
TGP6	22.06	TGP_S1	af	A	6.6	65.4	13.9	270	15	3	179.6	-33.0	10.5	257.6	-65.5
TGP5	22.31	TGP_S1	af	A	-	-	-	270	30	5	196.5	-48.5	12.0	205.8	-71.4
TGP4	22.53	TGP_S1	af	D	64.7	57.8	10.8	-	-	-	-	-	-	-	-
TGP3	22.71	TGP_S1	af	A	330.2	50.8	6.0	270	30	4	176.8	-29.1	18.3	263.5	-62.9
TGP2	22.91	TGP_S1	af	D	-	-	-	-	-	-	-	-	-	-	-
TGP1	22.98	TGP_S1	af	A	-	-	-	240	10	3	193.4	-43.6	13.1	219.6	-69.7
TGP103	23.13	TGP_S8	th	C	24.4	74.2	5.4	270	420	3	112.2	-45.8	25.6	354.3	-33.8
TGP102	23.56	TGP_S8	af	A	32.2	75.9	5.8	270	25	5	322.1	47.9	16.8	155.2	56.7
TGP101	23.91	TGP_S8	af	A	-	-	-	270	30	5	319.7	68.7	4.9	200.3	61.5
TGP97	25.68	TGP_S8	th	C	27.8	73.4	23.0	270	360	3	313.5	71.4	29.3	207.7	57.5
TGP95	26.08	TGP_S8	th	D	196.9	70.9	35.2	-	-	-	-	-	-	-	-
TGP94	26.85	TGP_S8	th	C	319.0	48.0	37.6	240	330	4	141.9	-35.8	24.4	323.4	-50.8
TGP92	27.45	TGP_S8	th	A	343.7	48.3	11.4	270	420	3	144.4	-24.5	13.8	313.5	-47.3
TGP90	28.04	TGP_S8	th	C	-	-	-	270	420	3	208.1	-58.9	21.0	164.9	-68.7
TGP86	29.20	TGP_S8	af	D	-	-	-	-	-	-	-	-	-	-	-
TGP84	30.15	TGP_S8	th	D	9.5	66.6	5.7	-	-	-	-	-	-	-	-
TGP126	30.85	TGP_S9	th	D	284.3	30.7	17.3	-	-	-	-	-	-	-	-
TP125	31.29	TGP_S9	th	A	327.9	64.8	10.0	270	360	4	339.9	16.5	18.8	109.9	51.6
TGP122	32.68	TGP_S9	af	D	9.2	65.3	3.3	-	-	-	-	-	-	-	-
TGP119	34.03	TGP_S9	th	D	43.9	39.4	5.2	-	-	-	-	-	-	-	-
TGP117	34.56	TGP_S9	th	D	345.6	72.0	22.1	-	-	-	-	-	-	-	-
TGP116	34.95	TGP_S9	th	D	48.4	33.7	12.2	-	-	-	-	-	-	-	-
TGP113	35.75	TGP_S9	th	D	346.2	53.4	7.5	-	-	-	-	-	-	-	-
TGP110	36.50	TGP_S9	af	D	332.7	60.6	6.4	-	-	-	-	-	-	-	-
TGP197	38.53	TGP_S13	th	D	202.9	50.8	29.5	-	-	-	-	-	-	-	-
TGP193	39.66	TGP_S13	th	D	158.5	4.3	35.2	-	-	-	-	-	-	-	-
TGP190	40.53	TGP_S13	th	A	194.7	38.5	8.4	150	300	5	156.4	-54.1	7.9	331.4	-70
TGP189	41.09	TGP_S13	th	A	220.1	42.1	9.9	240	390	4	181.1	21.9	11.4	255.4	-36.1
TGP187	41.44	TGP_S13	th	A	47.2	31.6	29.3	200	560	9	190.4	-64.8	7.0	133.3	-81.5
TGP186	41.66	TGP_S13	th	A	318.5	46.5	5.6	200	390	5	140.8	-50.0	14.4	339.1	-56.8
TGP183	42.64	TGP_S13	th	D	345.4	60.6	3.7	-	-	-	-	-	-	-	-
TGP182	42.89	TGP_S13	th	C	230.2	74.1	10.4	300	450	3	335.1	30.4	29.1	123.4	56.3
TGP180	43.24	TGP_S13	th	A	340.9	51.3	31.7	420	560	3	148.9	-45.4	16.2	325.1	-60.3

TGP250	81.09	TGP_S20	af	A	94.9	78.2	17.4	200	20	6	195.1	-43.4	11.2	216.1	-68.8
TGP251	81.49	TGP_S20	th	D	354.7	50.1	6.8	-	-	-	-	-	-	-	-
TGP252	82.07	TGP_S20	th	D	9.8	64.3	1.7	-	-	-	-	-	-	-	-
TGP253	82.62	TGP_S20	th	A	336.0	55.1	4.2	270	390	5	350.4	46.5	9.3	107.7	73.3
TGP254	83.1	TGP_S20	af	A	2.6	53.9	2.1	270	70	10	352.8	30.5	13.9	92.2	63.2
TGP256	84.14	TGP_S20	th	D	331.4	48.3	14.4	-	-	-	-	-	-	-	-
TGP261	84.81	TGP_S21	th	D	315.9	51.6	13.5	-	-	-	-	-	-	-	-
TGP260	85.41	TGP_S21	af	A	9.4	68.7	3.4	200	30	8	194	-45.6	9.0	215.8	-70.8
TGP258	86.03	TGP_S21	th	A	337.3	51.1	5.3	150	520	12	136.1	-39.2	7.7	331.7	-48.3
TGP257	86.65	TGP_S21	th	A	347.2	48.6	4.9	200	390	6	118.9	-43.6	7.8	348.3	-37.7
TGP262	88.62	TGP_S22	th	D	5.6	69.7	4.6	-	-	-	-	-	-	-	-
TGP263	88.72	TGP_S22	th	D	7.0	61.9	6.2	-	-	-	-	-	-	-	-
TGP267	91.3	TGP_S22	th	A	18.6	62.3	6.7	240	330	4	165.9	-32.2	10.0	286.6	-62.2
TGP268	91.78	TGP_S22	th	A	345.1	75.6	8.4	150	300	5	185.2	-57.4	11.5	213.5	-84
TGP269	92.38	TGP_S22	af	A	25.5	69.4	2.0	240	40	8	148.3	-20.2	16.7	306.8	-47.7
TGP270	92.62	TGP_S22	th	D	345.8	63.9	15.4	-	-	-	-	-	-	-	-
TGP273	94.04	TGP_S22	th	A	84.4	40.0	4.1	270	520	9	203.1	-41.3	14.8	203.9	-63.2
TGP275	94.94	TGP_S22	th	D	43.1	74.6	2.7	-	-	-	-	-	-	-	-
TGP277	95.94	TGP_S23	th	A	6.6	84.7	4.1	200	300	3	124.7	-44.7	16.4	345.3	-42.5
TGP278	96.34	TGP_S23	th	A	7.0	54.8	2.5	200	480	9	186.7	-39.4	7.0	239.1	-69.1
TGP280	97.84	TGP_S23	th	D	22.5	63.6	0.7	-	-	-	-	-	-	-	-
TGP281	98.54	TGP_S23	af	A	346.2	64.1	2.1	200	15	4	194.2	-67.3	7.8	124	-77.6
TGP283	99.89	TGP_S23	th	A	340.6	71.2	5.2	270	420	6	170.4	-36.8	10.1	279.8	-66.6
TGP284	100.59	TGP_S23	th	A	11.9	61.6	2.3	240	450	8	173.8	-41.7	9.8	274.2	-70.8
TGP285	101.31	TGP_S23	af	A	358.7	75.5	0.9	240	10	4	193	-11.7	14.7	235.6	-51.6
TGP286	102.23	TGP_S23	af	A	17.4	66.1	2.6	200	20	7	180.4	-47.7	3.4	255.2	-76.3
TGP288	103.68	TGP_S23	th	A	295.5	76.5	8.6	200	360	5	174	-40.8	18.7	273.2	-70.2
TGP289	104.28	TGP_S23	th	A	344.5	71.5	3.9	270	390	5	331.9	20.3	12.7	122.4	49.7
TGP290	105.03	TGP_S23	th	D	35.4	57.1	7.1	-	-	-	-	-	-	-	-
TGP291	105.63	TGP_S23	th	D	28.2	66.4	2.4	-	-	-	-	-	-	-	-
TGP293	107.02	TGP_S23	af	A	6.1	73.9	1.3	5	100	9	182.9	-75.8	19.9	80.4	-69.3
TGP294	108.06	TGP_S23	th	C	310.0	71.1	3.3	240	580	11	217.2	24.9	30.3	216.3	-24.8
TGP295	108.45	TGP_S23	th	A	356.9	65.9	5.2	270	390	5	312.3	57.8	12.0	176.7	54
TGP296	108.92	TGP_S23	af	D	300.5	74.1	3.2	-	-	-	-	-	-	-	-
TGP297	109.28	TGP_S23	th	C	334.3	71.6	5.4	270	520	6	276.3	51.6	28.8	188.2	25.4
TGP298	110.03	TGP_S23	th	A	17.9	69.0	4.4	270	420	6	325.1	29.4	9.0	135.5	49.9
TGP301	112.48	TGP_S23	af	C	4.2	68.1	8.4	270	60	9	249.3	59.2	31.8	209.2	13.6
TGP302	113.32	TGP_S23	th	C	11.7	61.5	7.1	270	580	7	108.2	42.6	28.3	316.6	4.2
TGP303	114.67	TGP_S23	th	C	30.6	35.5	4.2	270	480	7	118.5	23.9	32.4	317.8	-11.4
TGP304	115.38	TGP_S23	th	C	37.7	59.1	6.4	200	480	8	124.1	19.8	30.8	315	-16.7
TGP308	118.36	TGP_S24	th	A	62.3	70.6	2.9	150	560	12	156.3	-38.2	9.7	307.4	-61.1
TGP310	119.86	TGP_S24	th	A	1.5	68.3	1.4	200	330	5	142.5	-37.1	6.5	323.8	-51.8
TGP311	121.06	TGP_S24	th	A	329.8	68.6	2.0	150	520	7	150.2	-35.4	11.5	313.6	-56
TGP312	122.31	TGP_S24	th	A	21.1	73.3	1.0	200	360	5	183.2	-24.8	12.5	250.4	-60.4
TGP314	124.06	TGP_S24	th	A	23.2	66.3	5.2	150	390	7	171.6	-39.2	6.1	278.4	-68.5

TGP316	125.66	TGP_S24	th	D	356.9	66.3	1.6	-	-	-	-	-	-	-	-	-
TGP317	126.36	TGP_S24	th	A	343.1	78.8	7.7	200	480	9	145.9	-59.2	7.9	352.7	-64.4	
TGP319	127.56	TGP_S24	th	A	0.6	68.0	2.5	200	300	4	221.9	-39.8	17.9	183	-50	
TGP320	128.46	TGP_S24	th	A	5.6	56.5	1.7	200	480	10	164.7	-52.3	6.3	313.2	-74.6	
TGP321	129.64	TGP_S24	th	D	356.0	59.9	5.0	-	-	-	-	-	-	-	-	-
TGP322	130.09	TGP_S24	th	A	8.8	54.0	13.4	200	450	9	183.8	-55.5	6.4	231	-82.9	
TGP323	130.99	TGP_S24	th	A	20.2	61.1	7.4	270	420	7	46.5	78.9	6.2	283.9	54.5	
TGP324	132.24	TGP_S24	th	A	331.8	54.0	5.5	270	620	9	295.7	55.1	19.2	181.3	40.8	
TGP325	133.03	TGP_S24	th	A	32.8	75.6	9.3	270	520	8	358.4	65	11.6	243.1	85.4	
TGP326	134.48	TGP_S24	th	A	346.2	68.8	1.1	270	360	4	309.2	59.4	8.5	180.9	52.4	
TGP328	135.88	TGP_S24	th	A	29.9	55.3	4.7	270	480	6	354.1	74.3	13.0	247.6	71.5	
TGP329	137.03	TGP_S24	th	A	1.5	55.1	3.9	270	480	8	1.8	51	6.1	68.6	79.1	
TGP330	137.83	TGP_S24	th	A	9.1	62.8	2.7	270	580	10	7.2	53.5	7.7	40.6	79.8	
TGP331	138.93	TGP_S24	th	A	11.8	65.2	3.2	270	520	9	29.5	68.1	8.9	313	68.2	
TGP332	140.03	TGP_S24	th	A	3.8	67.4	1.6	270	520	8	309.8	61	3.9	183.5	53.4	
TGP333	140.88	TGP_S24	th	A	12.6	37.1	10.5	270	520	8	17.1	41.9	5.6	33.7	66.9	
TGP334	141.23	TGP_S24	th	A	5.7	57.7	4.7	270	580	10	1.6	54.9	6.4	66.2	82.8	
TGP335	141.53	TGP_S24	th	A	18.4	56.3	2.6	270	480	8	21.3	25.7	10.6	37.9	55.7	

Table S5. Summary of magnetic reversal ages and associated uncertainties from the WRG, UMB, ATPS06 and PEAT records. Metre levels for the ATPS06 are based on the compilation of Westerhold et al., 2012. Metre levels for the PEAT record are not specified, instead stratigraphic uncertainties are based on Table 1 of Westerhold et al., 2014. Stratigraphic uncertainties for the WRG and UMB records are derived from mean sediment accumulation rates calculated based on the age models of Sahy et al. (2015, 2017). U-Pb model uncertainties are outputs from the respective U-Pb calibrated age models, and are based upon the analytical uncertainties of the underpinning U-Pb dates. Astro model uncertainties are the uncertainties related to the tuning of the ATPS06 and PEAT models, and are assumed to be ± 0.05 Myr. U-Pb systematic uncertainties relate to the ^{238}U decay constant ($\pm 0.11\%$) and the calibration of the EARTHTIME isotopic trace ($\pm 0.03\%$). Astro systematic uncertainties are assumed to be $\pm 0.1\%$. Total age uncertainties are calculated based on Equations S1 - S4.

Magnetic reversal Section	Metre level	Reference	Age (Ma)	Stratigraphic uncertainty (2σ Myr)						$\pm 2\sigma$ total (Myr)
				$\pm 2\sigma$ U-Pb model (Myr)	$\pm 2\sigma$ U-Pb systematic (Myr)	$\pm 2\sigma$ Astro model (Myr)	$\pm 2\sigma$ Astro systematic (Myr)			
White River Group										
BC12n	Toadstool Geological Park	130.54 this study		31.275	0.016	0.146	0.036	-	-	0.166
TC13n	Toadstool Geological Park	65.62 this study		33.293	0.020	0.120	0.038	-	-	0.146
BC13n	Toadstool Geological Park	45.88 this study		33.688	0.075	0.130	0.038	-	-	0.211
TC15n	Flagstaff Rim	147.91 this study		34.825	0.014	0.086	0.040	-	-	0.109
BC15n	Flagstaff Rim	128.38 this study		34.988	0.005	0.110	0.040	-	-	0.122
TC16n.1n	Flagstaff Rim	76.13 this study		35.366	0.008	0.042	0.040	-	-	0.066
BC16n.1n	Flagstaff Rim	43.01 this study		35.633	0.034	0.060	0.041	-	-	0.106
TC16n.2n	Flagstaff Rim	20.97 this study		35.808	0.003	0.052	0.041	-	-	0.069
Umbria-Marche basin										
BC12n	Monte Cagnero	148.2 Coccioni et al. 2012		31.230	0.037	0.072	0.036	-	-	0.117
TC13n	Monte Cagnero	124.2 Coccioni et al. 2012		33.100	0.031	0.059	0.038	-	-	0.101
BC13n	Monte Cagnero	117.3 Coccioni et al. 2012		33.740	0.041	0.124	0.038	-	-	0.171
TC15n	Massignano	11.1 Jovane et al. 2007		34.910	0.005	0.058	0.040	-	-	0.075
BC15n	Massignano	9.3 Jovane et al. 2007		35.110	0.009	0.057	0.040	-	-	0.079
TC16n.1n	Massignano	6.2 Jovane et al. 2007		35.430	0.004	0.029	0.040	-	-	0.054
BC16n.1n	Massignano	5.5 Jovane et al. 2007		35.500	0.059	0.029	0.040	-	-	0.109
TC16n.2n	Massignano	3.3 Jovane et al. 2007		35.680	0.082	0.057	0.041	-	-	0.152
ATPS06										
BC12n	N/A	204.45 Pälike et al. 2006		31.034	0.004	-	-	0.050	0.031	0.062
TC13n	N/A	233.88 Pälike et al. 2006		33.157	0.003	-	-	0.050	0.033	0.063
BC13n	N/A	240.29 Pälike et al. 2006		33.705	0.001	-	-	0.050	0.034	0.061
TC15n	N/A	246.98 Pälike et al. 2006		35.126	0.007	-	-	0.050	0.035	0.068
BC15n	N/A	247.52 Pälike et al. 2006		35.254	0.048	-	-	0.050	0.035	0.110
TC16n.1n	N/A	247.94 Pälike et al. 2006		35.328	0.009	-	-	0.050	0.035	0.071
BC16n.1n	N/A	249.13 Pälike et al. 2006		35.554	0.007	-	-	0.050	0.036	0.068
TC16n.2n	N/A	249.45 Pälike et al. 2006		35.643	0.004	-	-	0.050	0.036	0.065
Pacific Equatorial Age Transect										
BC12n	N/A	- Westerhold et al. 2014		30.977	0.016	-	-	0.050	0.031	0.075
TC13n	N/A	- Westerhold et al. 2014		33.214	0.002	-	-	0.050	0.033	0.062
BC13n	N/A	- Westerhold et al. 2014		33.726	0.008	-	-	0.050	0.034	0.068
TC15n	N/A	- Westerhold et al. 2014		35.102	0.032	-	-	0.050	0.035	0.093
BC15n	N/A	- Westerhold et al. 2014		35.336	0.017	-	-	0.050	0.035	0.078
TC16n.1n	N/A	- Westerhold et al. 2014		35.580	0.015	-	-	0.050	0.036	0.076
BC16n.1n	N/A	- Westerhold et al. 2014		35.718	0.022	-	-	0.050	0.036	0.083
TC16n.2n	N/A	- Westerhold et al. 2014		35.774	0.021	-	-	0.050	0.036	0.082